Physics of Plasmas ARTICLE scitation.org/journal/php

Transverse beam envelope structures in strongly coupled stimulated Brillouin scattering

Cite as: Phys. Plasmas **27**, 102707 (2020); doi: 10.1063/5.0010872
Submitted: 15 April 2020 · Accepted: 20 September 2020 ·
Published Online: 14 October 2020

H. Schmitz,[a] R. Trines, and R. Bingham

AFFILIATIONS

Appleton Laboratory, Chilton, Didcot, Oxon OX11 0QX, United Kingdom

[a]Author to whom correspondence should be addressed: holger.schmitz@stfc.ac.uk

ABSTRACT

We use a newly developed code to investigate cross beam energy transfer via Brillouin scattering in the strong coupling limit. The code couples a single fluid model of the plasma to the complete set of Maxwell's equations. The code can describe beam interaction at arbitrary angles. We observe that the formation of a transverse structure on both beams is caused when the pump beam is fully depleted within the width of the beam. We present a simplified envelope model that confirms the results of the simulation. This transverse beam structure formation has implications for short pulse amplification. The results may also be relevant for fast ignition schemes for inertial confinement fusion.

The interaction of two or more laser beams in the presence of a plasma is a topic that is receiving growing interest. It is relevant, among others, for plasma-based amplifiers,[1–4] cross beam energy transfer (CBET) in inertial confinement fusion (ICF),[5–7] and the creation of transient photonic crystals.[8] In the context of pulse amplification, a plasma wave couples to the electromagnetic modes and transfers energy from a long pump beam to a short seed pulse. In the case of stimulated Raman scattering (SRS), the EM waves couple through an electron plasma wave,[3,9,10] and in the case of stimulated Brillouin scattering (SBS), the coupling is through an ion acoustic wave (IAW).[4] While pulse amplification through SRS has been found to suffer from limitations due to electron trapping and wave breaking,[3,11] amplification via SBS has recently gained increasing interest, especially in the strong coupling regime, because wave breaking is greatly reduced in this case.[12–14] CBET for direct drive and indirect drive typically takes place at laser intensities that correspond to the weak coupling SBS limit,[15–17] and at densities near the target at which SRS is suppressed.[10] However, strong coupling SBS may be important in the shock ignition scheme for ICF,[18] where peak laser intensities can reach several 10^{16} W/cm^2.

Traditionally, simulations of SBS use one of two approaches. In the envelope approximation, the laser field is separated into a rapidly oscillating carrier wave and a slowly varying envelope.[19] The introduction of a spatial envelope means that the model acquires a defined axial direction. In the paraxial approximation, laser propagation is limited to small angles in the axial direction. In the context of CBET, most simulations based on the envelope approximation additionally consider the strong damping limit.[20,21] Recently Myatt[22] presented simulations in which the damping is deemed appropriate for typical direct-drive experiments—which is about 10% of the real frequency. This could be considered strong, but the strong damping approximation was not used and therefore the response of the ions is not instantaneous. In Ref. 22, the ion-acoustic density perturbations, described by a second order differential equation in time, do not instantaneously follow the laser amplitude, but it does describe strong coupling physics.[23] In this work, we present a simulation model that includes damping without making the strong damping assumption. For the beam intensities considered here, the strong coupling dominates damping and, when the ion temperature is less than the electron temperature, Landau damping can be neglected altogether.

In order to capture a more complete picture of the physics of SBS, particle-in-cell (PIC) simulations can be used.[12,24] However, due to the numerical cost of PIC simulations, these investigations are limited to one-dimensional systems or very small simulation domains. In addition, PIC simulations add numerical noise which makes the interpretation of the results harder.

In this contribution, we use a newly developed hydro-code that includes the laser beams with a full Maxwell field solver to investigate cross-beam energy transfer in the strong coupling regime. We find that two laser beams intersecting at right angles not only transfer

energy, but also imprint a transverse structure onto each other. Similar structures are well known in the context of Brillouin or Raman amplification,[3,12,25] but appear there only in the longitudinal direction. We show that the structures are formed once the seed beam is able to completely deplete the pump beam on a scale length smaller than the pump diameter. Transverse beam structure formation has implications for short pulse amplification in the strong coupling SBS regime. It may also be relevant for CBET in shock ignition schemes where laser beams have high intensities during the shock acceleration phase.

In Sec. I, we present the basic equations and the simulation model. Section II presents the simulation results. In order to isolate the specific process of transverse beam structuring in the strong coupling, weak damping limit, we present results for an idealized geometry. While the conditions in different types of applications may be more involved, we believe that the results presented here may be relevant for short pulse amplification as well as fast ignition schemes. In Sec. III, we derive a semi-analytical model of the energy transfer between two orthogonal beams in the strong coupling, weak damping limit. Section IV contains the conclusions.

I. SIMULATION MODEL

We implemented a 2D code to simulate the plasma response to crossing laser beams and the influence of the plasma on the laser propagation. In contrast to previous codes,[21,22] we do not use an envelope model for the laser beams, nor do we linearize the plasma equations. Especially, the latter can be important when the density perturbations grow to become comparable to the equilibrium density. The plasma will be modeled by a single fluid description. In order to derive this model, we start from the general two fluid description of a plasma,

$$\partial_t n_s + \nabla \cdot (n_s \mathbf{v}_s) = 0, \tag{1}$$

$$m_s \partial_t (n_s \mathbf{v}_s) + \nabla \cdot [m_s n_s \mathbf{v}_s \mathbf{v}_s + p_s] = n_s q_s (\mathbf{E} + \mathbf{v}_s \times \mathbf{B}) + \mathbf{R}_s. \tag{2}$$

Here, the index $s = e, i$ represents the fluid species. Multiplying the continuity equations (1) for each species by their respective masses m_e and m_i and adding them, provides us with the mass continuity equation

$$\partial_t \rho + \nabla \cdot (\rho \mathbf{v}) = 0. \tag{3}$$

Here, $\rho = m_i n_i + m_e n_e$ is the mass density and $\mathbf{v} = (m_i n_i \mathbf{v}_i + m_e n_e \mathbf{v}_e)/\rho$ is the mass flow velocity. Adding the momentum equations (2) for each species, the electric field terms cancel exactly due to the assumption of quasineutrality $n_e = Z n_i$. The combined momentum equation then reads

$$\partial_t (\rho \mathbf{v}) + \nabla \cdot [\rho \mathbf{v}\mathbf{v} + p] + Z m_e n (\mathbf{v}_e \cdot \nabla) \mathbf{v}_e = \mathbf{j}_e \times \mathbf{B} - \nu \rho \mathbf{v}. \tag{4}$$

This equation also assumes that the electric current $\mathbf{j}$ is carried mostly by the light electrons $\mathbf{j} \approx \mathbf{j}_e$. In the derivation of these equations, no temporal averaging was carried out. This means that all quantities retain their full time dependence. The pressure is assumed to be dominated by the electrons, $p \approx p_e$, assuming that the ion temperature is small. We assume the electrons to be adiabatic. In the remainder of this article, we will be restricting ourselves to a two-dimensional geometry in which the seed beams are s-polarized. Under these assumptions the electric field and hence the fast electron quiver motion is directed perpendicular to the simulation plane. As a result, the last term on the LHS of Eq. (4) vanishes exactly in our choice of polarization.

These equations are simulated using the central upwind scheme by Kurganov *et al.*[26] In this flux conservative scheme, the quantities ρ and $\mathbf{v}$ are given on the cell centers. Their time derivatives are determined by evaluating the fluxes on the cell boundaries. Time integration is then carried out using a third-order Runge–Kutta scheme.

The equation for the electron current is obtained from Eq. 2. Assuming that the main driver of the electron current is the transverse oscillating electric field, we can neglect the spatial derivatives. Also, the influence of the magnetic field is small compared to the electric field for non-relativistic electrons. We end up with the Drude model for the electron current.

$$\frac{\partial \mathbf{j}_e}{\partial t} = \frac{Z e^2}{m_e m_i} \rho \mathbf{E} - \gamma \mathbf{j}_e. \tag{5}$$

This is a local equation that can be directly integrated using the same Runge–Kutta scheme as above. The coefficient γ is the damping coefficient for the electron current in the fast electromagnetic field. Unlike the strong damping limit, we do not place restrictions on the damping coefficients and the plasma density is allowed to evolve freely in time through Eqs. (3) and (4). We note that there are, of course, limitations on the type of damping that can be described stemming from the nature of the hydrodynamic model. We assume in the following that kinetic effects such as Landau damping can be neglected. The electron current enters the equations only in the calculation of the $\mathbf{j}_e \times \mathbf{B}$ force on the plasma and in Ampère's law. Note again that Eq. (4) results from adding the electron and ion momentum equation and assuming quasineutrality. Hence, the force from the electrons on the ions through the electric field is contained implicitly in the momentum equation. The resulting equations model the effect of the ponderomotive force on the electrons, and since we are considering the ion timescale, also the bulk plasma. The equations are thus capable of describing the generation of ion sound waves. Due to the assumption of quasineutrality, the equations exclude Langmuir waves. Note that, by neglecting the $\mathbf{j}_e \times \mathbf{B}$ term in Eq. (5), we are assuming that the electron current is purely transverse. In an exact description, there will be a small contribution in the longitudinal direction due to the ponderomotive force. Most of the longitudinal electron current will, however, be canceled out by an equivalent ion current that maintains quasineutrality. The error made by this approximation is of the order $k\lambda_D \ll 1$. The electromagnetic field equations are

$$\nabla \times \mathbf{E} = -\frac{\partial \mathbf{B}}{\partial t}, \tag{6}$$

$$\nabla \times \mathbf{B} = \frac{1}{c^2} \frac{\partial \mathbf{E}}{\partial t} + \mu_0 \mathbf{j}_e, \tag{7}$$

where the contribution of the ion current density has been neglected. These fields are advanced using the standard Finite Difference Time Domain (FDTD) scheme on the Yee grid.[27] This is a standard method,[28] also widely used in many PIC simulations.[29,30] We stress here again that we are solving the full set of Maxwell's equations without reverting to an envelope model. The boundaries are assumed to be absorbing and modeled using a perfectly matched layer.[31] More details on this particular implementation of the FDTD solver can be found in Schmitz and Mezentsev.[32]

At this point, a few remarks about the model equations (3)–(7) are in order. Maxwell's equations (6) and (7) describe the full evolution

of the electromagnetic field. In the case of two overlapping beams with frequencies ω_1 and ω_2, both **E** and **B** will contain both beam frequencies as well as the beat frequency $(\omega_1 - \omega_2)/2$. The $\mathbf{j}_e$ in Ampère's law, Eq. (7), accounts for the electron current and, together with Eq. (5), the dispersion for electromagnetic modes in the plasma are recovered. In the region of overlapping beams, $\mathbf{j}_e$ will also contain the beam frequencies and the beat frequency since it is linearly driven by the electric field. Then, the $\mathbf{j}_e \times \mathbf{B}$ term subsequently is a non-linear driver for the bulk plasma motion that contains both the sum frequency $\omega_1 + \omega_2$ as well as the difference frequency $\omega_1 - \omega_2$. The latter of these can drive slow ion acoustic modes that are responsible for Brillouin scattering. The ion acoustic modes create periodic density fluctuations that, in turn, create periodic modifications of the dispersion relation for electromagnetic waves through the electron current equation (5). These are then the cause for the scattering of the electromagnetic waves from one beam into the other. We conclude that the model presented here contains all necessary physics to describe Brillouin scattering. We have carried out numerical tests and confirmed that the code recovers both the dispersion relation for electromagnetic waves as well as the dispersion relation for ion acoustic modes. Due to the nature of the single-fluid model, any kinetic effects have been neglected. This implies that the model will naturally break down once the wave breaking limit is reached.

II. SIMULATION RESULTS

The simulation is initialized with a homogeneous plasma at rest with a density of $n_e = 0.3 n_{\text{crit}}$, where n_{crit} is the critical density for the laser wavelength $\lambda_0 = 0.351\,\mu$m. The choice of n_e suppresses any Raman scattering which cannot exist for densities $n_e > n_{\text{crit}}/4$. The pump beam is injected along the x-axis. It has an intensity of 6.5×10^{15} W cm^{-2}. The seed beam, injected along the y-axis, has an intensity of 5×10^{14} W cm^{-2}. Both beams have a half-width of 30 μm and a rise time of 10 μm/c. The rise time corresponds to a bandwidth of $\Delta\omega \approx 2 \times 10^{13}$ s^{-1}. This bandwidth is almost ten times larger than the frequency of the ion acoustic wave at $\lambda_i = \lambda_0/2$ of $\omega_i \approx 3.4 \times 10^{12}$ s^{-1}. For this reason, the pump and the seed beam can exchange energy through Brillouin scattering, even though they have identical frequencies and do not meet the matching conditions precisely. The seed is injected with a delay of 20 μm/c as compared to the pump. The beams are s-polarized with respect to the simulation domain. For these simulations, we neglect any damping of the ions, $\nu = 0$. Assuming that the ion temperature is less than the electron temperature, $T_i < T_e$, Landau damping of the ion wave can be neglected.[9] A small damping rate of the electromagnetic wave, $\gamma = 10^{-3}\omega_{pe}$, has been included mainly for numerical stability. The resulting simulation required about 500 CPU hours for a system of 3800^2 grid cells.

Figure 1 shows the out of plane electric field during the interaction of the two beams. At a simulation time of $t = 1.75$ ps, the beams have just crossed. The beating of the two beams has not yet had a chance to noticeably affect the plasma density and the beams propagate without a change in their amplitude. At $t = 2.5$ ps, energy transfer from the pump to the seed beam due to Brillouin scattering can be observed. The amplification of the seed beam reaches saturation as the pump is depleted. One can observe that only the leftmost part of the seed beam is amplified. This is due to the fact that the depletion of the pump beam takes place on a scale length that is shorter than the width of the seed. At $t = 3.5$ ps, the amplified portion of the seed moves further

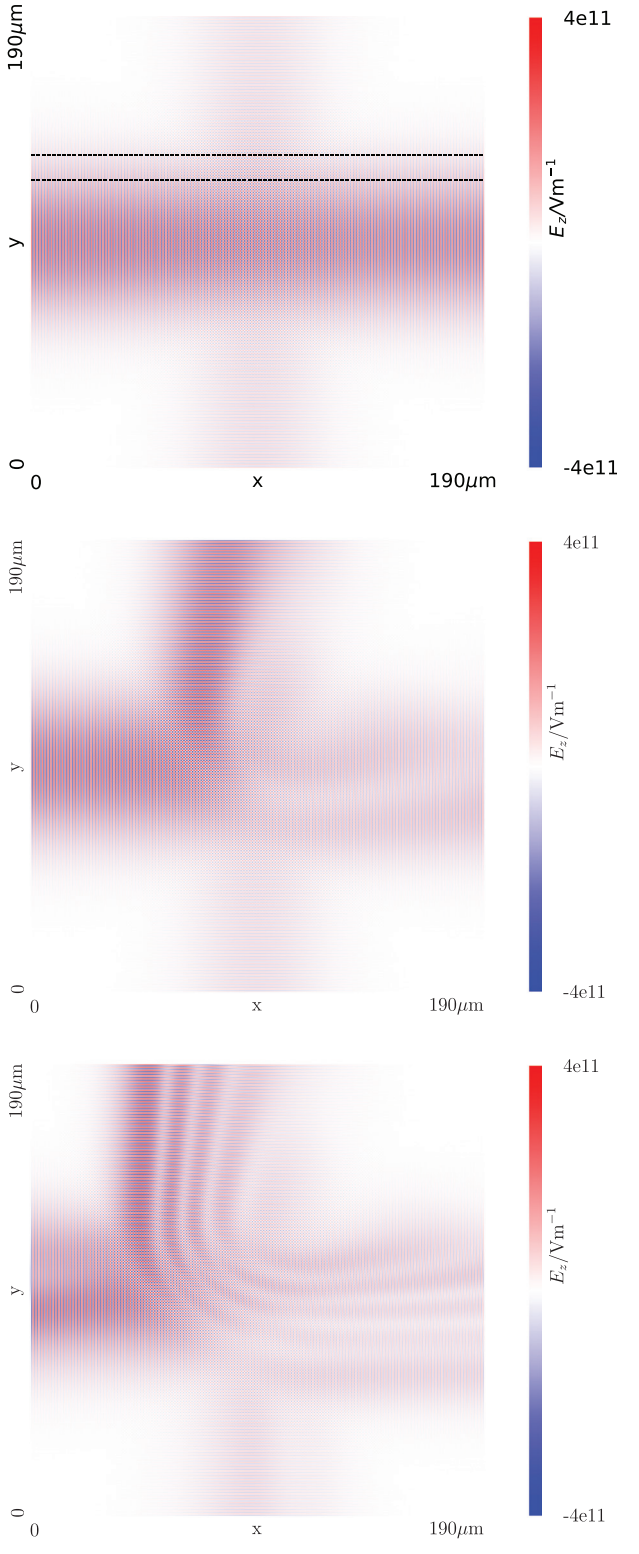

FIG. 1. The out of plane electric field at times $t = 1.75$ ps (top panel), $t = 2.5$ ps (middle panel), and $t = 3.5$ ps (bottom panel).

upstream with relation to the pump beam. A regular structure of the amplified beam perpendicular to the propagation direction is observed. This pattern is mirrored in the downstream pump beam which shows a similar modulation perpendicular to its propagation direction. It should be noted that similar patterns can be seen in the simulation results presented by Lancia *et al.*,[33] but were not discussed there.

Figure 2 shows a line out of the amplitude along the x-axis for the times $t = 2.5$ ps, 3 ps, and 3.5 ps. The amplitude has been averaged over a 10 μm interval in the y-direction from $y = 125\,\mu$m to $y = 135\,\mu$m as indicated in the top panel of Fig. 1 by the dashed lines. This slice is well outside the pump beam and clearly shows the transverse amplitude variation of the seed beam as it leaves the interaction region. The transverse profile exhibits a multi-peaked structure. As time advances, the height of the peaks increases and the width decreases. In addition to this, the peaks move to the left and new, smaller peaks start appearing on the right. As the seed beam gathers energy and increases in amplitude, it eventually fully depletes the pump pulse. Where the pump is depleted and the seed has gained maximum energy, the roles of pump and seed reverse and energy is transferred back into the pump. Thus, the energy oscillates back and forth between the pump and seed. Shortly after the times shown here at about 4 ps, the amplitude of the density perturbation grows to match the absolute value of the plasma density. At this time, we expect wave breaking to occur and the single-fluid model to break down.

Within the interaction region, one can observe that the electric field structures are elongated and curved, approximately along the hyperbolic contours $xy =$ const, given a suitable coordinate origin. This will be exploited in the semi-analytical theory developed in Sec. III. Outside the interaction region, the structures appear to bend in on themselves, away from the axes. This can be explained by the free propagation of the features once they leave the interaction region and are no longer modified.

III. ANALYTICAL MODEL

We now provide a semi-analytical theory of the initial growth based on the envelope appropriation for the electromagnetic fields. The theory presented here has superficial similarities to the analysis of cross beam interaction by McKinstrie *et al.*[34,35] Here, the amplification

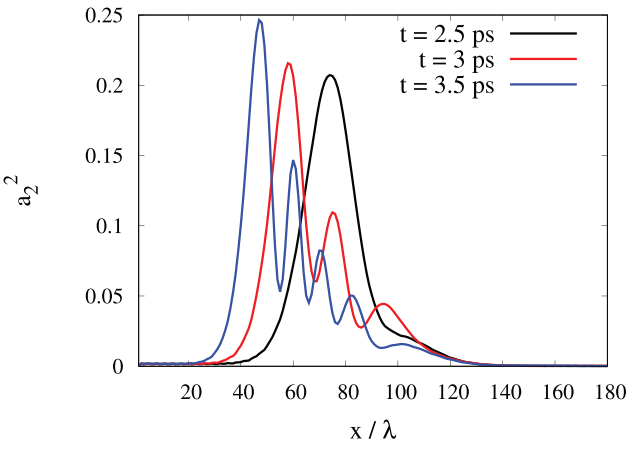

FIG. 2. The normalized amplitude along the x-axis from the full-wave simulation for the times $t = 2.5$ ps, 3 ps, and 3.5 ps.

of a seed beam by a pump intersecting at arbitrary angles was investigated. However, in those investigations, the focus was mainly on time-independent solutions in which collisions limited the growth of the instability. In contrast, we focus on the rapid time evolution of the density in the strong coupling regime. This evolution takes place on a timescale that is comparable to or smaller than the ion acoustic period.

The coupled wave equations for Brillouin scattering are

$$\begin{aligned}\omega\partial_t\mathbf{A_1} + c^2(\mathbf{k_1}\cdot\nabla)\mathbf{A_1} &= \frac{\omega_{pe}^2}{4n_0}\tilde{n}\mathbf{A_2},\\ \omega\partial_t\mathbf{A_2} + c^2(\mathbf{k_2}\cdot\nabla)\mathbf{A_2} &= -\frac{\omega_{pe}^2}{4n_0}\tilde{n}^*\mathbf{A_1},\\ \partial_t^2\tilde{n} + c_s^2k_3^2\tilde{n} &= -in_0k_3^2\frac{Ze^2}{mm_i}\mathbf{A_1}\mathbf{A_2^*}.\end{aligned} \tag{8}$$

Here, $\mathbf{A_1}$ and $\mathbf{A_2}$ are the envelopes of the vector potential of the pump beam and the seed beam, respectively, $\mathbf{A_i} \to \mathbf{A_i}\exp(i(\mathbf{k}_i\cdot\mathbf{x} - \omega_i t))$. The plasma ion density n is split into a constant background and a small variation, $n = n_0 + \tilde{n}\exp(i\mathbf{k}_3\cdot\mathbf{x})$. By making this approximation, the model presented here will capture only the initial linear growth of the density perturbation. It turns out that this is sufficient to explain the transverse beam structures observed in the simulations. Note, that $\tilde{n}$ is the envelope of the density perturbation in space only and still contains the full time dependence. The three waves have wave vectors $\mathbf{k_i}$ and frequencies ω_i with $i = 1$ for the pump beam, $i = 2$ for the seed beam, and $i = 3$ for the ion acoustic wave. The frequency of the ion plasma wave is small compared to the frequencies of the laser beams. This allows the approximations $\omega_1 \approx \omega_2 = \omega$ and $|\mathbf{k_1}| \approx |\mathbf{k_2}| = k$. Assuming that the pump beam propagates in the positive x-direction and the seed beam in the positive y-direction, the coupling conditions for the wave vectors read, $\mathbf{k_1} = \mathbf{k_2} + \mathbf{k_3}$

$$\mathbf{k_1} = k\hat{\mathbf{x}}, \tag{9}$$

$$\mathbf{k_2} = k\hat{\mathbf{y}}, \tag{10}$$

$$\mathbf{k_3} = k(\hat{\mathbf{x}} - \hat{\mathbf{y}}), \tag{11}$$

where $\hat{\mathbf{x}}$ and $\hat{\mathbf{y}}$ are the coordinate vectors. Inserting this into equation (8) gives

$$\omega\partial_t\mathbf{A_1} + c^2k\partial_x\mathbf{A_1} = \frac{\omega_{pe}^2}{4n_0}\tilde{n}\mathbf{A_2}, \tag{12}$$

$$\omega\partial_t\mathbf{A_2} + c^2k\partial_y\mathbf{A_2} = -\frac{\omega_{pe}^2}{4n_0}\tilde{n}^*\mathbf{A_1}, \tag{13}$$

$$\partial_t^2\tilde{n} + 2c_s^2k^2\tilde{n} = -2in_0k^2\frac{Ze^2}{mm_i}\mathbf{A_1}\mathbf{A_2^*}. \tag{14}$$

In the strong coupling regime, the second term on the left-hand side of Eq. (14) is small compared to the first and can be dropped. We introduce normalized quantities

$$\begin{aligned}\tau &= \frac{1}{T}t, \quad \xi,\eta = \frac{\omega}{c^2kT}x,y,\\ n &= \frac{T\omega_{pe}^2}{4n_0\omega}\tilde{n}, \quad \mathbf{a}_j = \frac{e}{m_ec}\mathbf{A}_j; \quad j = 1,2,\\ T &= \left(\frac{2\omega m_i}{Zm\omega_{pe}^2k^2c^2}\right)^{1/3}.\end{aligned} \tag{15}$$

The equations can then be written as

$$\begin{aligned} \partial_\tau a_1 + \partial_\xi a_1 &= n a_2, \\ \partial_\tau a_2 + \partial_\eta a_2 &= -n^* a_1, \\ \partial_\tau^2 n &= -i a_1 a_2^*. \end{aligned} \tag{16}$$

In the results of the numerical simulations, we have seen that the features in the interaction region are elongated along the hyperboles $xy = \text{const}$. This suggests that hyperbolic coordinates might provide a good description of the problem. We use the transformed coordinates

$$\xi = v \exp(-u), \quad \eta = v \exp(u). \tag{17}$$

The v-coordinate maps onto the radial lines ($u = \text{const}$), while the u-coordinate maps onto the hyperboles ($v = \text{const}$). In this system, we can neglect derivatives along u. Any variation in this direction is much slower that the variation across the hyperboles in the v-direction. Neglecting ∂_u with respect to ∂_v does not mean that the solution does not depend on u. However, it allows us to integrate the equations for each value of u independently. With this, the equations simplify to

$$\partial_\tau a_1 + \exp(u)\partial_v a_1/2 = n a_2, \tag{18}$$

$$\partial_\tau a_2 + \exp(-u)\partial_v a_2/2 = -n^* a_1, \tag{19}$$

$$\partial_\tau^2 n = -i a_1 a_2^*. \tag{20}$$

For a given u, Eqs. (18)–(20) can be solved numerically using standard techniques. The quantities a_1, a_2, and n are stored on a numerical grid in v. The derivatives with respect to v are calculated using finite differences. Then, the integration with respect to τ is carried out using a standard fourth order Runge–Kutta scheme. For comparison, we use the same parameters as those in the 2D simulation. The normalized beam amplitudes are calculated from the on-axis peak amplitudes of the Gaussian beams in the simulation, $a_{1,0} = 2.42 \times 10^{-2}$ and $a_{2,0} = 6.71 \times 10^{-3}$. These amplitudes are used as boundary conditions for Eqs. (18) and (19) at $v = 0$. Figure 3 shows a plot of the intensity a_2 at $\eta = 8.12$ as a function of ξ for different times. For each pair of η and ξ, the values of u and v are calculated from Eq. (17). Equations (18)–(20) are then integrated for the given u and evaluated at v.

The beam amplitudes in Fig. 3 show the same transverse structure as seen in the numerical results shown in Fig. 2. There are, however, several differences between the model and the full simulation which are due to the nature of the model. The simulations show a smooth rise of the intensity from $x = 0$ to the location of the peak. The model does not capture this slope due to the boundary conditions in the model that assume a perfect step transverse beam profile. This means that, in the model, the peak intensity is located at $\xi = 0$. The growth of the peak intensity is overestimated in the model during the times shown in the figure. At these times, the density perturbations in the simulation are nearing saturation. The model contains a linearized approximation of the density perturbation that cannot capture the saturation. As time progresses, we can observe the same increase in the initial peak and the development of new, smaller peaks to the right of the leading peak. Figure 4 shows a plot of the maximum intensity of the seed beam over time. The results from the simulation are shown by the black curve, denoted the *Gaussian Beam* and the model is shown by the blue curve. In order to determine the analytical growth rate of the leading peak of the seed beam, we have to evaluate Eqs. (18)–(20) at $\xi = 0$ by taking the limit $u \to \infty$. Equation (18) immediately gives $\partial_v a_1 = 0$ or $a_1 = a_{1,0}$. This makes intuitive sense as the pump beam propagates in the ξ direction and has not yet interacted with the seed beam at $\xi = 0$. In this limit, Eqs. (19) and (20) can be reduced to $\partial_\tau^3 a_2 = -i|a_1|^2 a_2$. This equation has three solutions, one of which has a positive growth rate of $\lambda = (\sqrt{3} + i)/2|a_1|^{2/3}$, in agreement with linear analysis, e.g., Ref. 10. This growth has been plotted in Fig. 4 as a dashed line. The model agrees well with the analytical result. The simulation shows a much-decreased growth that saturates quickly. The differences can be understood in terms of the transverse Gaussian beam shape in the simulation. The growth rate has been calculated using the peak amplitude of the pump beam. In the simulation, the seed beam will mostly encounter lower amplitudes while traversing the pump, thus reducing the overall growth rate. In addition, it was observed that the peak of the amplified beam gradually moves left

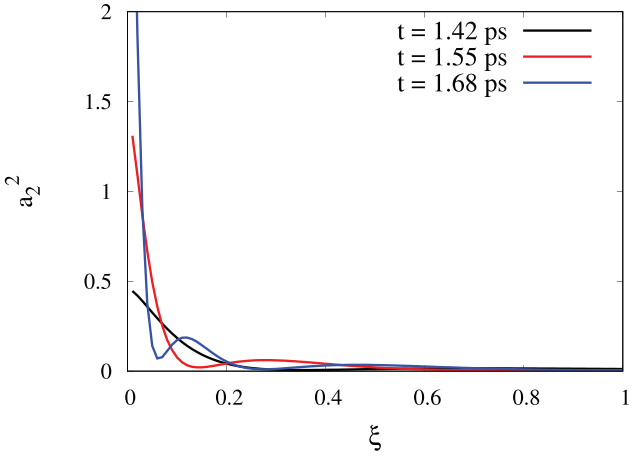

FIG. 3. The normalized amplitude along the ξ-axis resulting from the model, Eqs. (18)–(20), for the times $t = 1.42$ ps, 1.55 ps, and 1.68 ps.

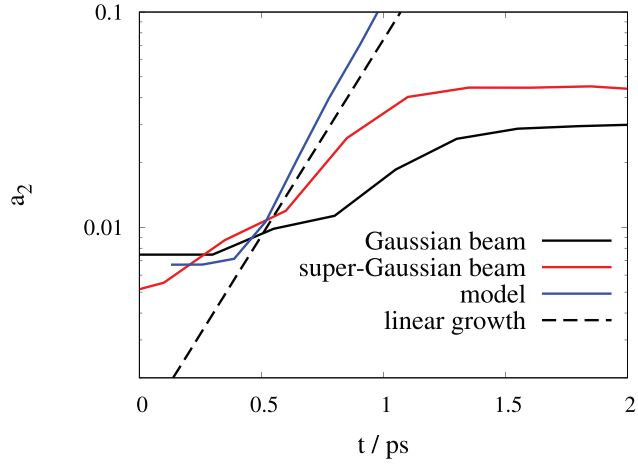

FIG. 4. The peak amplitude a_2 of the seed beam over time for the simulation and the model. The curve for the simulation has been shifted left by 0.7 ps in order to align with the locations of maximum growth of the two plots.

during the simulation. At each point in time, a different part of the seed contributes to the growth curve, and the initial amplitude of this part decreases over time. Both effects depend on the transverse beam shapes and should reduce when a more top-hat like beam profile is used. To corroborate this finding, we have repeated the simulation with a super-Gaussian beam with an order of $n = 8$. The resulting growth rate is plotted as the red curve in Fig. 4. It can be clearly seen that the maximum growth rate is approaching the analytical growth rate in this case.

IV. CONCLUSIONS

Using a novel simulation code, we have shown that energy exchange between crossing beams in the strong coupling SBS regime is susceptible to transverse beam structuring. Traditional numerical treatment of stimulated Brillouin scattering in plasmas has used either envelope approximation models or full particle in cell simulations. Using a full Maxwell solver coupled to a fluid model of the plasma, we were able to investigate the strong coupling SBS interaction of two laser beams intersecting at a right angle. We observed previously unreported structuring of both pump and seed beams perpendicular to the direction of propagation. These structures may have implications for a range of topics in laser–plasma applications, such as plasma optics, cross-beam energy transfer, or short pulse amplification.

The transverse pulse profile is reminiscent of the π-pulse in the weak coupling regime and similar to the pulse profile in pulse amplification via strong coupling SBS. In our case, however, the pulse profile does not propagate with the seed beam, but instead is fixed in space at the position of the beam intersection. We developed an analytical theory which underlines the similarity between the observed transverse structures and the longitudinal peaks observed in short pulse amplification.

DATA AVAILABILITY

The data that support the findings of this study are available from the corresponding author upon reasonable request.

REFERENCES

[1]M. Maier, W. Kaiser, and J. A. Giordmaine, "Intense light bursts in the stimulated Raman effect," Phys. Rev. Lett. **17**, 1275–1277 (1966).
[2]R. D. Milroy, C. E. Capjack, and C. R. James, "Plasma laser pulse amplifier using induced Raman or Brillouin processes," Phys. Fluids **22**, 1922 (1979).
[3]V. Malkin, G. Shvets, and N. Fisch, "Fast compression of laser beams to highly overcritical powers," Phys. Rev. Lett. **82**, 4448–4451 (1999).
[4]R. D. Milroy, C. E. Capjack, and C. R. James, "A plasma-laser amplifier in the 11-16μm wavelength range," Plasma Phys. **19**, 989–995 (1977).
[5]C. J. Randall, J. R. Albritton, and J. J. Thomson, "Theory and simulation of stimulated Brillouin scatter excited by nonabsorbed light in laser fusion systems," Phys. Fluids **24**, 1474 (1981).
[6]P. Michel, L. Divol, E. Williams, C. Thomas, D. Callahan, S. Weber, S. Haan, J. Salmonson, N. Meezan, O. Landen, and S. Dixit, "Energy transfer between laser beams crossing in ignition hohlraums," Phys. Plasmas **16**, 042702 (2009).
[7]W. Kruer, S. Wilks, B. Afeyan, and R. Kirkwood, "Energy transfer between crossing laser beams," Phys. Plasmas **3**, 382–385 (1996).
[8]G. Lehmann and K. H. Spatschek, "Laser-driven plasma photonic crystals for high-power lasers," Phys. Plasmas **24**, 056701 (2017).
[9]J. F. Drake, P. K. Kaw, Y. C. Lee, G. Schmidt, C. S. Liu, and M. N. Rosenbluth, "Parametric instabilities of electromagnetic waves in plasmas," Phys. Fluids **17**, 778 (1974).
[10]D. Forslund, J. M. Kindel, and E. L. Lindman, "Theory of stimulated scattering processes in laser-irradiated plasmas," Phys. Fluids **18**, 1002–1016 (1975).
[11]M. S. Hur, R. R. Lindberg, A. E. Charman, J. S. Wurtele, and H. Suk, "Electron kinetic effects on Raman backscatter in plasmas," Phys. Rev. Lett. **95**, 115003 (2005).
[12]A. A. Andreev, C. Riconda, V. T. Tikhonchuk, and S. Weber, "Short light pulse amplification and compression by stimulated Brillouin scattering in plasmas in the strong coupling regime," Phys. Plasmas **13**, 053110 (2006).
[13]E. Guillaume, K. Humphrey, H. Nakamura, R. M. G. M. Trines, R. Heathcote, M. Galimberti, Y. Amano, D. Doria, G. Hicks, E. Higson, S. Kar, G. Sarri, M. Skramic, J. Swain, K. Tang, J. Weston, P. Zak, E. P. Alves, R. A. Fonseca, F. Fiúza, H. Habara, K. a Tanaka, R. Bingham, M. Borghesi, Z. Najmudin, L. O. Silva, and P. A. Norreys, "Demonstration of laser pulse amplification by stimulated Brillouin scattering," High Power Laser Sci. Eng. **2**, e33 (2014).
[14]J.-R. Marquès, L. Lancia, T. Gangolf, M. Blecher, S. Bolaños, J. Fuchs, O. Willi, F. Amiranoff, R. L. Berger, M. Chiaramello, S. Weber, and C. Riconda, "Joule-level high-efficiency energy transfer to subpicosecond laser pulses by a plasma-based amplifier," Phys. Rev. X **9**, 021008 (2019).
[15]D. Turnbull, A. Colaïtis, R. K. Follett, J. P. Palastro, D. H. Froula, P. Michel, C. Goyon, T. Chapman, L. Divol, G. E. Kemp, D. Mariscal, S. Patankar, B. B. Pollock, J. S. Ross, J. D. Moody, E. R. Tubman, and N. C. Woolsey, "Crossed-beam energy transfer: Polarization effects and evidence of saturation," Plasma Phys. Controlled Fusion **60**, 054017 (2018).
[16]R. K. Kirkwood, D. P. Turnbull, T. Chapman, S. C. Wilks, M. D. Rosen, R. A. London, L. A. Pickworth, W. H. Dunlop, J. D. Moody, D. J. Strozzi, P. A. Michel, L. Divol, O. L. Landen, B. J. MacGowan, B. M. VanWonterghem, K. B. Fournier, and B. E. Blue, "Plasma-based beam combiner for very high fluence and energy," Nat. Phys. **14**, 80–84 (2018).
[17]I. V. Igumenshchev, D. H. Edgell, V. N. Goncharov, J. A. Delettrez, A. V. Maximov, J. F. Myatt, W. Seka, A. Shvydky, S. Skupsky, and C. Stoeckl, "Crossed-beam energy transfer in implosion experiments on OMEGA," Phys. Plasmas **17**, 122708 (2010).
[18]L. J. Perkins, R. Betti, K. N. Lafortune, and W. H. Williams, "Shock ignition: A new approach to high gain inertial confinement fusion on the National Ignition Facility," Phys. Rev. Lett. **103**, 045004 (2009).
[19]W. L. Kruer, *The Physics of Laser Plasma Interactions* (Westview Press, Inc., 2003).
[20]J. F. Myatt, A. V. Maximov, W. Seka, R. S. Craxton, and R. W. Short, "Modeling stimulated Brillouin scattering in the underdense corona of a direct drive inertial confinement fusion target," Phys. Plasmas **11**, 3394–3403 (2004).
[21]D. J. Marion, A. Debayle, P. E. Masson-Laborde, P. Loiseau, and M. Casanova, "Modeling crossed-beam energy transfer for inertial confinement fusion," Phys. Plasmas **23**, 052705 (2016).
[22]J. F. Myatt, R. K. Follett, J. G. Shaw, D. H. Edgell, D. H. Froula, I. V. Igumenshchev, and V. N. Goncharov, "A wave-based model for cross-beam energy transfer in direct-drive inertial confinement fusion," Phys. Plasmas **24**, 056308 (2017).
[23]J. F. Myatt, J. G. Shaw, R. K. Follett, D. H. Edgell, D. H. Froula, J. P. Palastro, and V. N. Goncharov, "LPSE: A 3-D wave-based model of cross-beam energy transfer in laser-irradiated plasmas," J. Comput. Phys. **399**, 108916 (2019).
[24]K. A. Humphrey, R. M. Trines, F. Fiuza, D. C. Speirs, P. Norreys, R. A. Cairns, L. O. Silva, and R. Bingham, "Effect of collisions on amplification of laser beams by Brillouin scattering in plasmas," Phys. Plasmas **20**, 102114 (2013).
[25]I. Y. Dodin, G. M. Fraiman, V. M. Malkin, and N. J. Fisch, "Amplification of short laser pulses by Raman backscattering in capillary plasmas," J. Exp. Theor. Phys. **95**, 625–638 (2002).
[26]A. Kurganov, S. Noelle, and G. Petrova, "Semidiscrete central-upwind schemes for hyperbolic conservation laws and Hamilton–Jacobi equations," SIAM J. Sci. Comput. **23**, 707–740 (2001).
[27]K. Yee, "Numerical solution of initial boundary value problems involving Maxwell's equations in isotropic media," Antennas and Propagation, IEEE Trans. Antennas Propag. **14**, 302 (1966).
[28]A. Taflove and S. Hagness, *Computational Electrodynamics*, 3rd ed. (Artech House, Boston/London, 2005).
[29]R. A. Fonseca, L. O. Silva, F. S. Tsung, V. K. Decyk, W. Lu, C. Ren, W. B. Mori, S. Deng, S. Lee, and T. Katsouleas, "OSIRIS: A three-dimensional, fully relativistic particle in cell code for modeling plasma based accelerators," in International Conference on Computational Science (2002), pp. 342–351.

[30]T. D. Arber, K. Bennett, C. S. Brady, A. Lawrence-Douglas, M. G. Ramsay, N. J. Sircombe, P. Gillies, R. G. Evans, H. Schmitz, a. R. Bell, and C. P. Ridgers, "Contemporary particle-in-cell approach to laser-plasma modelling," Plasma Phys. Controlled Fusion **57**, 113001 (2015).
[31]J. A. Roden and S. D. Gedney, "Convolution PML (CPML): An efficient FDTD implementation of the CFS–PML for arbitrary media," Microwave Opt. Technol. Lett. **27**, 334–339 (2000).
[32]H. Schmitz and V. Mezentsev, "Full-vectorial modeling of femtosecond pulses for laser inscription of photonic structures," J. Opt. Soc. Am. B **29**, 1208–1217 (2012).
[33]L. Lancia, J. R. Marquès, M. Nakatsutsumi, C. Riconda, S. Weber, S. Hüller, A. Mančić, P. Antici, V. T. Tikhonchuk, A. Héron, P. Audebert, and J. Fuchs, "Experimental evidence of short light pulse amplification using strong-coupling stimulated Brillouin scattering in the pump depletion regime," Phys. Rev. Lett. **104**, 025001 (2010).
[34]C. J. McKinstrie, J. S. Li, R. E. Giacone, and H. X. Vu, "Two-dimensional analysis of the power transfer between crossed laser beams," Phys. Plasmas **3**, 2686–2692 (1996).
[35]C. J. McKinstrie, V. A. Smalyuk, R. E. Giacone, and H. X. Vu, "Power exchange between crossed laser beams and the associated frequency cascade," Phys. Rev. E **55**, 2044–2047 (1997).